# Segregation-affected yielding and stability in nanotwinned silver by microalloying

Xing Ke[1] and Frederic Sansoz[1,2,*]

[1]*Materials Science Program, The University of Vermont, Burlington, Vermont 05405, USA*
[2]*Department of Mechanical Engineering, The University of Vermont, Burlington, Vermont 05405, USA*

Small-scale mechanics of solute atom segregation and incipient plasticity in nanotwinned Ag containing trace concentrations of Cu were studied by using large-scale hybrid Monte Carlo and molecular-dynamic simulations. It is found that solute Cu atoms are segregated concurrently to grain boundaries and intrinsic twin-boundary kink-step defects during thermal annealing. Low Cu dopant contents below 1 at. % are predicted to substantially increase twin stability in nanotwinned Ag, accompanied with a pronounced rise in yield strength at 300 K. Incipient plasticity is associated with kink-step migration, grain-boundary sliding, and dislocation nucleation from grain boundaries and twin-boundary defects, which are affected by doping. Cu-dependent yield strengthening in doped nanotwinned Ag is shown to correlate with the critical stress required to initiate crystal slip emitted from grain boundaries and twin-boundary defects. These findings provide fundamental insight into the roles of twin-boundary imperfections on plastic yielding, and offer clues to further extend the extraordinary stability and strength of nanotwinned metals by microalloying.

## I. INTRODUCTION

Nanotwinned (nt) metals consist of coherent twin boundaries (TBs) with nanometer-scale spacing, formed during film growth, plastic deformation, or thermal annealing [1]. nt-Cu metals have shown tensile strengths up to 10 times higher than that of conventional coarse-grained Cu [2], combined with lower electrical resistivity [3,4], higher structure stability [5], and higher corrosion resistance [6] than nanocrystalline (nc) and ultrafine-grained Cu. It is well accepted, both experimentally and theoretically, that the underpinning for strengthening in nt metals is the resistance of coherent TBs to lattice dislocation motion [7–10]. Also, recent evidence from experiments and atomistic simulations [11–13] has shown that TB defects in nt-Cu, such as nanoscale kinklike incoherent steps [14], play important roles in plastic deformation processes during dislocation-TB interactions and ductility. To date, however, it remains challenging to fundamentally understand and control how intrinsic TB imperfections contribute to plastic yielding in nt metals.

Microalloying by segregation of solute atoms to grain boundaries (GBs) has been studied extensively as an effective route for increasing both stability and yield strength in nc metallic alloys where conventional solid solution strengthening is generally absent [15–21]. The core principle is to diffuse low concentrations of solute atoms to crystalline interfaces by thermal annealing in order to either reduce the excess free energy (or volume) of the GB network [16,22] or form fine pinning precipitates inside GBs to resist grain growth [23]. Spectacular strengthening effects by GB microalloying have been achieved successfully in nanograined face-centered-cubic binary alloys with high segregation enthalpies, such as Nb-doped Cu [17,24], Ti-doped Ni [25], and Mg-doped Al [21]. In nc-Cu materials, Özerinç *et al.* [24] have experimentally reported a 120% increase in nanoindentation hardness with segregated solute Nb up to 10 at. %. At 1 at. % dilute atoms and above, however, it was shown that GBs thicken into zones

leading to phase separation and large elemental (Nb)-based precipitation [23], which was observed to adversely increase the electrical resistivity [26]. Similarly, Zhang *et al.* [19] have observed that segregating Zr atoms to 0.5 at. % increased hardness, ductility, and fatigue resistance in nc-Cu, but GB strength weakening was observed above 2 at. % Zr due to amorphous phase formation. Furthermore, different atomistic simulation studies in Ag-doped Cu alloys with sub-15-nm grain diameters [17,27] predicted that tensile yield strength increased linearly by 30% with Ag microalloying up to 1.5 at. %, before decreasing at high concentrations, due to Ag doping effects on GB free volume. One study [27], however, suggested that the strengthening efficiency by GB microalloying with Ag atoms was reduced at a larger grain size, i.e., 40 nm.

Despite rapid progress in nc metals, the influence of microalloying on strength and stability in nt metals remains largely unexplored. In this study, large-scale hybrid Monte Carlo and molecular-dynamics (MC/MD) simulations were performed to study atomic-scale segregation processes from microalloying in nt-Ag containing trace concentrations of Cu up to 0.8 at. %, and understand their roles in incipient yielding mechanisms. Experimentally, sputter-deposited Ag films are well known to form abundant nanotwins due to the low stacking-fault energy of this metal [28–30]. Our simulated nt-Ag samples were made of a relatively large grain size (45 nm) holding a high density of kinked or perfect nanotwins, like in those experiments. Remarkably, we find that Cu dopant is strongly segregated to TB kink defects during annealing, in addition to traditional GB doping, which dramatically enhances twin stability under high stress. Microalloying gives rise to nearly twofold increase in yield stresses with low elemental amounts of Cu (<1 at. %). The objective of this study is to determine the atomic mechanism(s) governing the dependence of yield strength on Cu dopant concentration.

## II. COMPUTATIONAL METHODS

Hybrid MC/MD simulations [22,31] were performed to structurally and chemically relax large-scale and small-scale
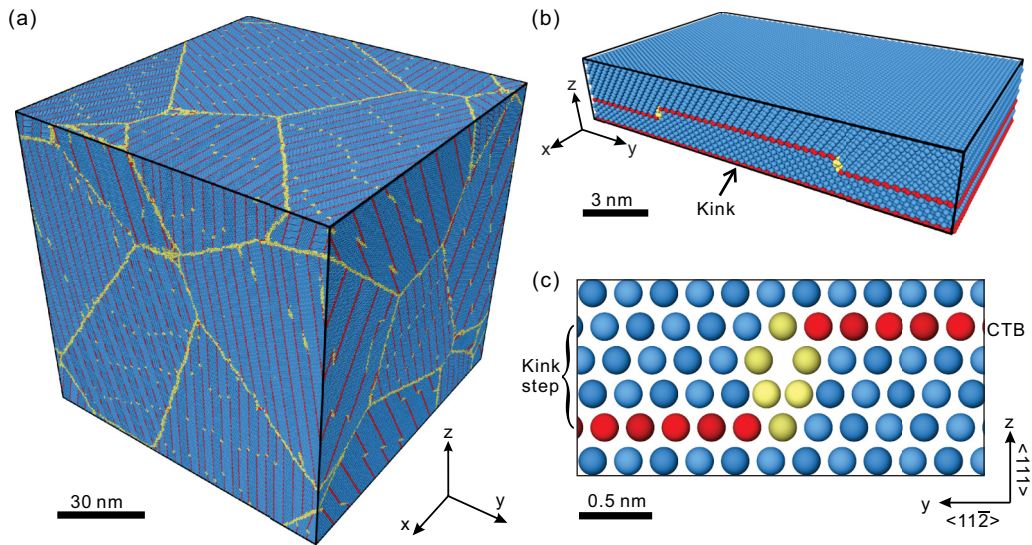
---

FIG. 1. Atomistic models used for simulations of solute atom segregation and tensile deformation in (a) nanotwinned Ag with kinked TBs of 2.8-nm thickness and an average grain size of 45 nm, and (b) nt-Ag bicrystal containing only one single TB kink defect. (c) Atomic structure in a TB kink step. Atoms in perfect fcc arrangement are colored in blue, coherent TBs in red color, GB and TB defects in yellow color.

nt-Ag models containing Cu dopant concentrations between 0 and 0.8 at. %. The software LAMMPS [32] was used with an embedded-atom method potential for Ag-Cu binary alloys by Wu and Trinkle [33]. This potential was fitted from *ab initio* data to match surface atom diffusivities and generalized stacking-fault energy curves in this system. Our own simulations with this potential showed that the unstable and stable stacking-fault energies in pure Ag were equal to 115.3 and 16.6 mJ/m$^2$, respectively. We found that the generalized stacking-fault energy curve remained unchanged by randomly adding Cu atoms up to 5 at. % concentration, which indicated that solid solution strengthening was absent. Large atomistic models of dimensions 90 nm × 90 nm × 90 nm were created in Ag with a total of 42.6 million atoms, as shown in Fig. 1(a). Seven grain regions of 45 nm in average diameter were created by a Voronoi tessellation scheme with randomly distributed grain centers, random crystallographic orientations, and fully periodic boundary conditions, similar to our previous work [34]. GB atoms closer than 0.5 Å were removed. Each grain contained constantly spaced TBs created by mirror-copying operation on the fcc stacking sequence along the [111] direction. A small TB spacing of 2.8 nm was used because the effect of microalloying on twin stability was expected to be more prominent with a smaller TB spacing, and this spacing is more vulnerable to detwinning through partial dislocation glide [8]. Two types of model comprising either kinked or perfect TBs were considered. Small-scale atomistic models consisted of a GB-free nt-Ag bicrystal containing one single TB kink, as shown in Fig. 1(b). Bicrystal models were 24 nm×4 nm×14 nm with periodic boundary conditions and 83 000 atoms. The atomic structure of each kink step was equivalent to repeating pattern $b_2 : b_1 : b_3$ of an incoherent $\Sigma 3\{112\}$TB, with Burgers vectors $b_1 = 1/6[\overline{11}2]$, $b_2 = 1/6[\overline{1}2\overline{1}]$, and $b_3 = 1/6[2\overline{11}]$, characterized by a zero sum [35]. The minimal energy configuration of a kink-step defect reached by the conjugate gradient method is shown in Fig. 1(c). Before MC/MD simulation, the steps in large-scale

models were uniformly distributed with a separation distance of 10 nm, following past observations made by transmission electron microscopy [11]. The step height was 0.7 nm.

The energy of each model was minimized by the conjugate gradient method. The structure was then relaxed under zero pressure using an isothermal-isobaric (NPT) ensemble at 450 K for 100 ps, then cooled to 300 K in 50 ps, and held at the same temperature for another 50 ps. Temperature was rescaled every 500 steps. The timestep was 5 fs, which was found to conserve the total system energy. The hybrid MC/MD approach used to simulate Cu atom segregation followed the method presented in Ref. [36]. Our goal was to simulate a thermal annealing process of relevance to past experiments in nt-Ag prepared using the magnetron sputtering technique [1]. In particular, vacuum annealing at a minimum temperature of 423 K was applied after sputtered deposition by Bufford *et al.* [37] to study the thermal stability of twins in nt-Ag. Therefore, our simulations were run at 500 K for 1 million MD steps with a timestep of 2 fs and calls to MC every ten MD steps. Temperature in MD was controlled by rescaling every ten steps and pressure was maintained to 0 bar using a Berendsen barostat. The MC simulation part was carried out with a chemical potential difference $\Delta\mu = -2.5$ eV, variance of Lagrange multiplier $\kappa = 100$, and target Cu concentrations of 0.2, 0.4, 0.6, and 0.8 (in at. %). The simulation output showed that standard deviation of Cu at. % was about $1.0 \times 10^{-5}$ and the acceptance ratio was close to $2.5 \times 10^{-6}$. After segregation, the models were relaxed again in the NPT ensemble under zero pressure from 500 to 300 K for 100 ps, and kept at 300 K for another 100 ps.

The large-scale models were deformed in pure tension by stretching the simulation boxes at an engineering strain rate of $10^8$ s$^{-1}$ along the $x$ direction until 3% strain. The NPT ensemble at 300 K and zero pressure applied laterally along the $z$ and $y$ directions was used. Bicrystal models were subjected to three different loading modes corresponding to shearing up to 10% strain on either $xy$, $xz$, or $yz$ planes, respectively. The

average tensile or shear stresses were computed by adding the corresponding virial-theorem stress component over all atoms, and dividing by the deformed volume of the simulation box. The 0.2% offset yield stress was determined by fitting the linear portion of the stress-strain curves up to the stress at which the first dislocations or GB plasticity were detected. Plastic

deformation mechanisms were studied by common neighbor analysis (CNA) and atomic strain analysis in the software OVITO [38]. A network of three-dimensional cells of ~1 nm in wall thickness encompassing each GB interface in the model was created by the Voronoi tessellation method [39] to identify a list of GB atoms before deformation. We did not use CNA
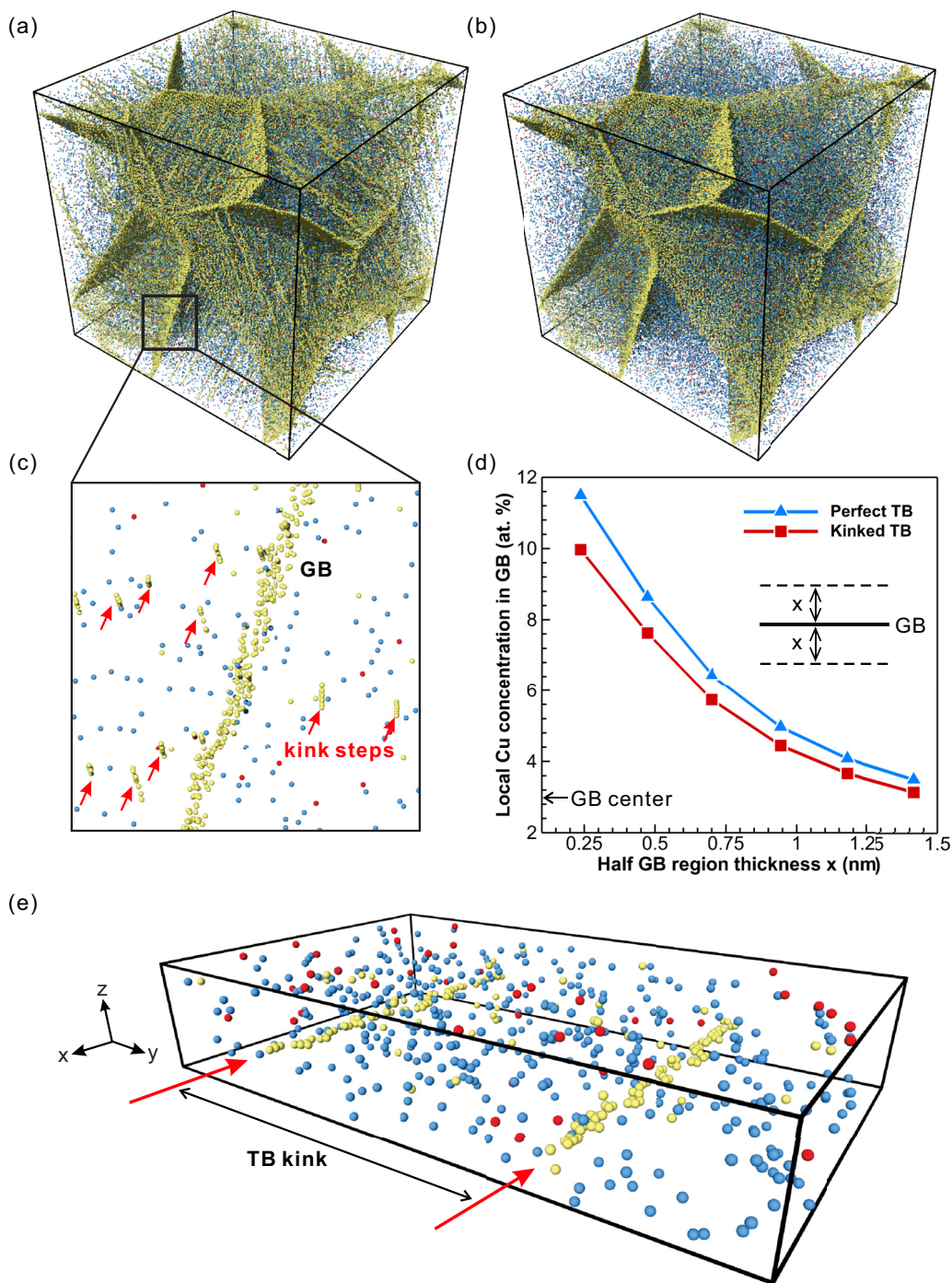


FIG. 2. Hybrid MC/MD simulations of segregation of 0.8 at. % Cu atoms in nanotwinned Ag during 500 K annealing. Equilibrium Cu atom distribution simulated in large-scale nt-Ag model containing (a) kinked TBs and (b) perfect TBs. (c) Close-up view of Cu segregation to GB and TB kink steps in a thin slice from (a). (d) Average local Cu concentration in GB region in (a) and (b). (e) Cu atom distribution (0.8 at. %.) after segregation in GB-free bicrystal model containing one kink defect. Cu atoms segregated to TB kink steps and GBs are colored in yellow, those moved to coherent TB segments in red, and other atoms staying in solution are in blue color. The original position of individual TB kink steps was indicated with a red arrow.

for GB atom detection, to avoid adding extra atoms from kink defects present inside the grains. The average atomic shear strain was calculated in the estimated GB network as a function of applied strain. The onset of GB plasticity was defined as the configuration reaching an average shear strain in GBs of 0.05, which was determined from detailed analysis of atomistic simulation snapshots at different strains. The simulations were performed on the high-performance SuperMIC supercomputer in the Extreme Science and Engineering Discovery Environment (XSEDE) [40].

## III. RESULTS

### A. Equilibrium Cu segregation in nanotwinned Ag

Equilibrium Cu atom distributions with Ag atoms deleted, as obtained after hybrid MC/MD simulations at a concentration of 0.8 at. % Cu, are shown in Figs. 2(a) and 2(b) for large-scale nt-Ag models with kinked and perfect TBs, respectively. In the model with perfect TBs, it is found in Fig. 2(b) that after thermal annealing, a large majority of Cu atoms are segregated to the GBs, with fewer Cu atoms in the grain interior. Dopant atoms left inside grains are randomly distributed at both face-centered-cubic and hexagonal-close-packed lattice sites, suggesting perfect alloying element dilution. By contrast, the model with kinked TBs in Fig. 2(a) shows evidence that a

significant fraction of dopants is attracted by intrinsic TB kink steps to form extended lines of Cu atoms inside the grains, alongside GB segregation.

A close-up view of a thin slice in Fig. 2(c) reveals that Cu atoms were not segregated to the coherent TB segments, but more preferentially to TB steps and GBs. Qualitatively, it appeared as if Cu doping was equal in both types of defect. Quantitatively, in Fig. 2(d) we estimated the local Cu concentration segregated in the three-dimensional GB network. Here the local dopant concentration in GB was calculated by using the ratio of Cu atoms over total number of Ag and Cu atoms in the GB network. Different values of half GB wall thickness $x$, as schematically shown in the inset of Fig. 2(d), were chosen from 0.24 to 1.4 nm by considering $x$ as multiples of the (111) interplanar distance in Ag. With perfect TBs and 0.8 at. % Cu concentration, the local Cu concentration near the GB center reached 11.5 at. %, suggesting that even in small amounts Cu dopants are strongly attracted by sites in the GB core. Interestingly, in the presence of TB defects such as kinks, Fig. 2(d) also reveals that the highest local Cu concentration in GB decreased to 10 at. %, indicating that atom segregation to TB kink steps inside the grain has become significant. We verified this hypothesis by simulating the process of Cu atom segregation in the GB-free bicrystal model [Fig. 1(b)], with an equivalent dopant concentration of
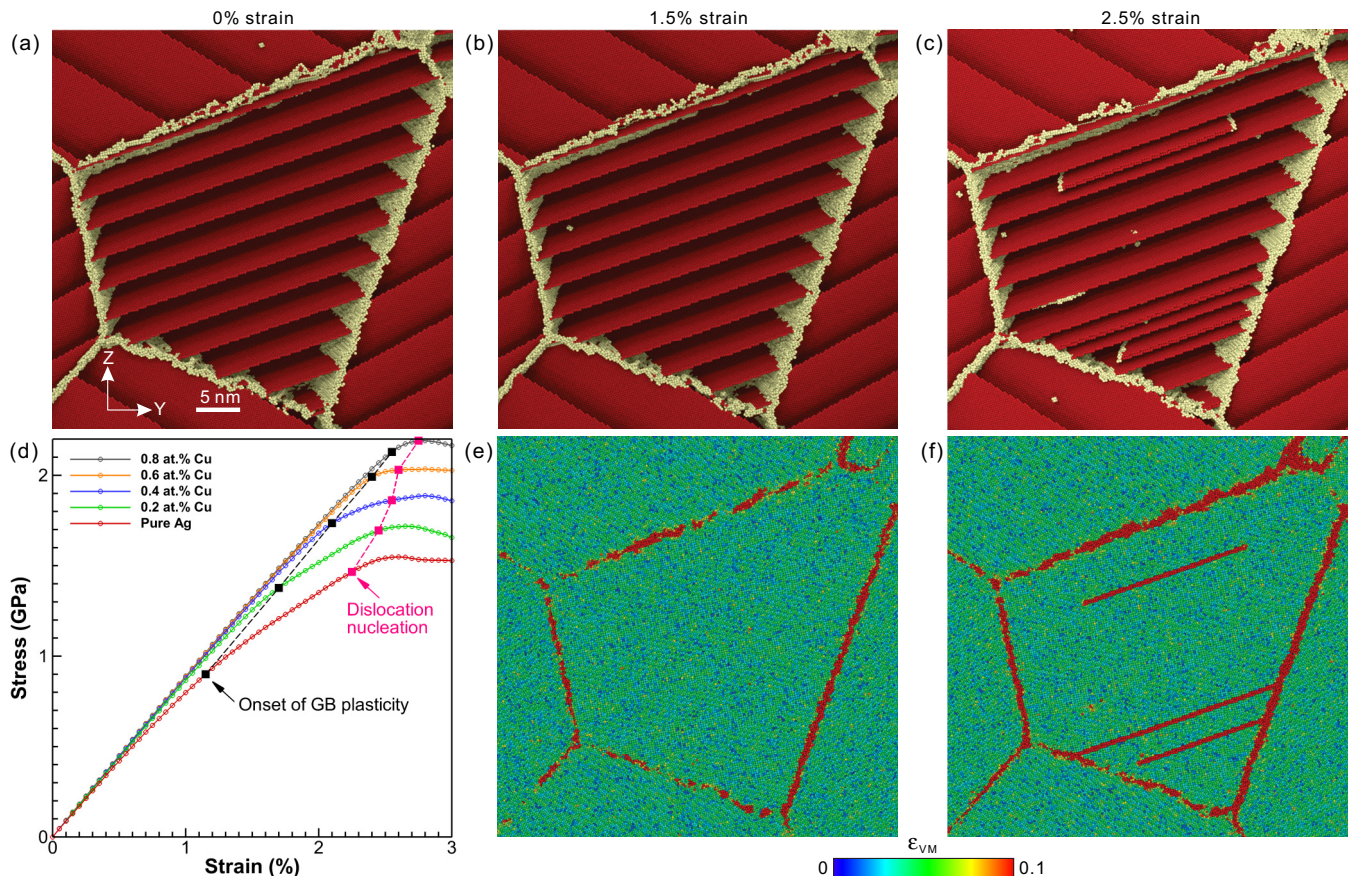


FIG. 3. Incipient plastic deformation mechanisms at 300 K in undoped and Cu-doped nanotwinned Ag containing perfect TBs. (a) Atomistic snapshots of microstructure in nt-Ag before deformation. Atoms in perfect fcc arrangement have been omitted for clarity. (d) Stress-strain curves at yielding with different Cu contents. Deformed microstructures and corresponding atomic von Mises shear-strain ($\varepsilon_{vm}$) distributions in undoped nt-Ag at (b),(e) 1.5% strain and (c),(f) 2.5% strain.
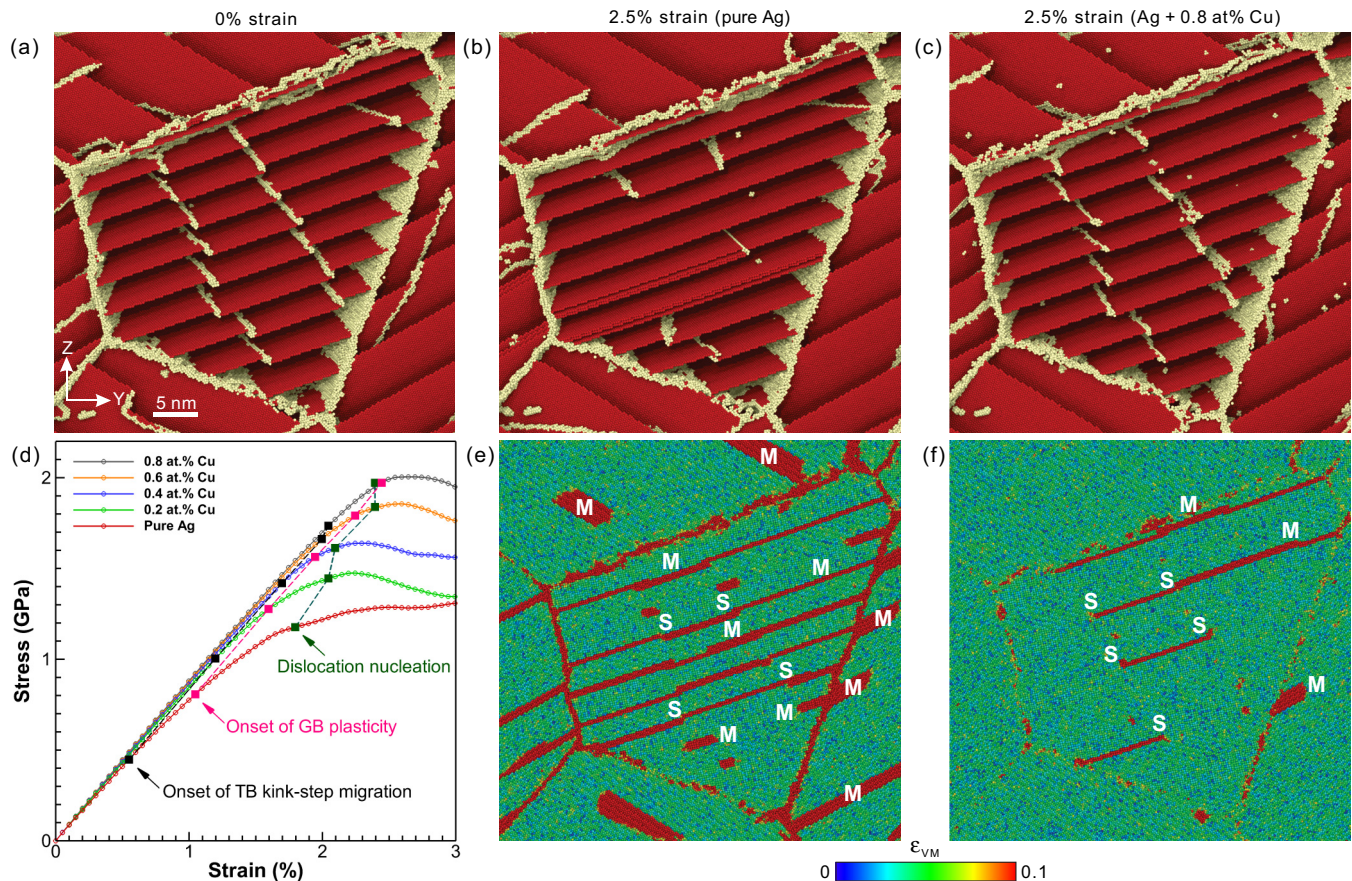
FIG. 4. Incipient plastic deformation mechanisms at 300 K in undoped and Cu-doped nanotwinned Ag containing kinked TBs. (a) Atomistic snapshots of microstructure in nt-Ag before deformation. Atoms in perfect fcc arrangement have been omitted for clarity. (d) Stress-strain curves at yielding with different Cu contents. Deformed microstructures and corresponding atomic von Mises shear-strain ($\varepsilon_{vm}$) distributions in undoped nt-Ag at (b),(e) 1.5% strain and (c),(f) 2.5% strain. M = detwinning by TB kink migration and S = dislocation nucleation by TB kink splitting.

0.8 at. % Cu. Figure 2(e) shows that most substitutional sites along the two TB kink steps are replaced by Cu atoms, and that the remainder of dopants stays randomly distributed in solution. No preferential segregation to coherent TB segments is found.

## B. Incipient plasticity mechanisms

To understand the effects of Cu dopant segregation on stability and yielding of doped nt-Ag, plasticity mechanisms around the yield point at 300 K were studied for different segregated Cu contents. First, incipient plastic deformation processes in a representative nt-Ag grain from the large-scale model containing perfect TBs are presented in Fig. 3 and Movie S1 provided as Supplemental Material [41]. GBs are found to be stable with limited migration during deformation up to 3% strain. In undoped nt-Ag, the onset of plastic deformation is characterized by GB plasticity in the form of interface sliding [Figs. 3(b) and 3(e)], followed by nucleation of extended partial dislocation loops from GBs [Fig. 3(c) and 3(f)]. Movie S1 clearly shows that all dislocation loops are emitted from GBs and propagate on (111) slip planes parallel to TBs. This result mostly agrees with the atomistic simulation study by Li *et al.* [8] in nt-Cu at small TB spacings, with the

exception that dislocation emission is distributed along GBs and not site-specific in nt-Ag, while it was always localized at GB-TB triple junctions in nt-Cu.

With Cu dopant addition, Movie S3 [41] shows significant improvement in microstructure stability up to 3% strain. Stress-strain curves shown in Fig. 3(d) indicate that the onset of GB plasticity always occurs before dislocation nucleation. It is observed, however, that the critical stresses at onsets of GB plasticity and dislocation nucleation increased substantially with Cu content, and that the stress difference between these two events is reduced tenfold as Cu content increases. Specifically, in nt-Ag doped with 0.8 at. % Cu, dislocation nucleation is rapidly initiated after the stress is augmented by 60 MPa above that for the first GB sliding event, in contrast to 600 MPa in its undoped equivalent.

Now, we shift attention to the stability and yielding of nt-Ag containing TB kink imperfections, as shown in Fig. 4(a) before deformation. Two atomistic simulation snapshots of the same grain deformed at 2.5% tensile strain in undoped and doped nt-Ag are compared in Figs. 4(b) and 4(c), respectively. In Figs. 4(b) and 4(e) and Movie S2 [41] depicting the behavior of pure nt-Ag, the majority of kink steps are shown to migrate easily along TBs under stress. Migrating kink steps are either merged with neighboring ones with opposite Burgers vectors

or absorbed into a nearby GB to produce perfectly coherent TB segments. Therefore, it is possible to regard kink migration as a lower limit of twin instability, since this process leads to detwinning. In Fig. 4(b) and Movie S2, several kink steps can be observed to dissociate into partial dislocations gliding independently along the supporting TB. This process involves the emission of one or two twin partial dislocations splitting from the initial $b_1 : b_2 : b_3$ kink step structure presented in Fig. 1(c). It is worth noting that kink migration is somewhat different from kink splitting, because the former involves motion of three $b_1 : b_2 : b_3$ partial dislocations altogether [13].

In the case of Cu-segregated nt-Ag models, Figs. 4(c) and 4(f) show that kink migration and splitting were both simulated, but the latter mechanism was significantly more dominant, as only a few kinks very close to GBs could be found to migrate and be absorbed under stress. It should be pointed out that in splitting, kink steps have been converted into new dislocation nucleation sites, consistent with recent experimental observations made in nt-Cu metals [12]. Therefore, these results show that the primary Cu segregation effect on plastic deformation mechanisms is to reduce twin instability by shifting from kink-step migration in pure nt-Ag to kink-mediated dislocation nucleation in doped nt-Ag, which is also confirmed by the bicrystal simulations below.

The dependence of yielding mechanisms on stress and Cu content in defective nt-Ag is summarized in Fig. 4(d). Incipient plasticity in this type of metal relates to kink-step migration, grain-boundary sliding, and dislocation nucleation from GBs and TB defects, which are affected by Cu dopant concentration. Importantly, Fig. 4(d) shows that kink migration takes place at much smaller stress than the onsets of GB plasticity and dislocation nucleation, at any Cu contents. Like nt-Ag with perfect TBs, however, the stress difference between plasticity events decreases dramatically with increasing Cu amounts, which provides evidence that microalloying has enhanced twin stability and yield strength in unison.

### C. Dependence of yield strength on Cu segregation

Critical stresses at the onsets of TB kink migration, GB sliding, and dislocation nucleation as functions of segregated Cu content are presented in Figs. 5(a) and 5(b) for perfect and kinked TBs, respectively. The 0.2% offset yield stresses determined from the stress-strain curves presented in Figs. 3(d) and 4(d) have been included for comparison. At the same Cu content, we find that offset yield stresses in doped nt-Ag are smaller with kinked TBs than with perfect ones. Yield strength relates to Cu concentration almost linearly. From 0 to 0.8 at. % Cu doping, yield stress in nt-Ag increases from 1.26 to 2.13 GPa (69% rise) in the presence of perfect TBs, and from 1.09 to 2.00 GPa (83% rise) with kinked ones. In addition, Fig. 5 confirms that Cu segregation affects the critical stress to activate each mechanism. Yet, the Cu dependence of offset yield strengths is found to match more closely the Cu dependence for the onset of dislocation nucleation for both perfect and imperfect TBs.

To further investigate the fundamental roles played by Cu segregation on the stability and yielding of intrinsic TB kink steps alone, plastic deformation mechanisms in GB-free bicrystals subjected to pure shear loading are presented in
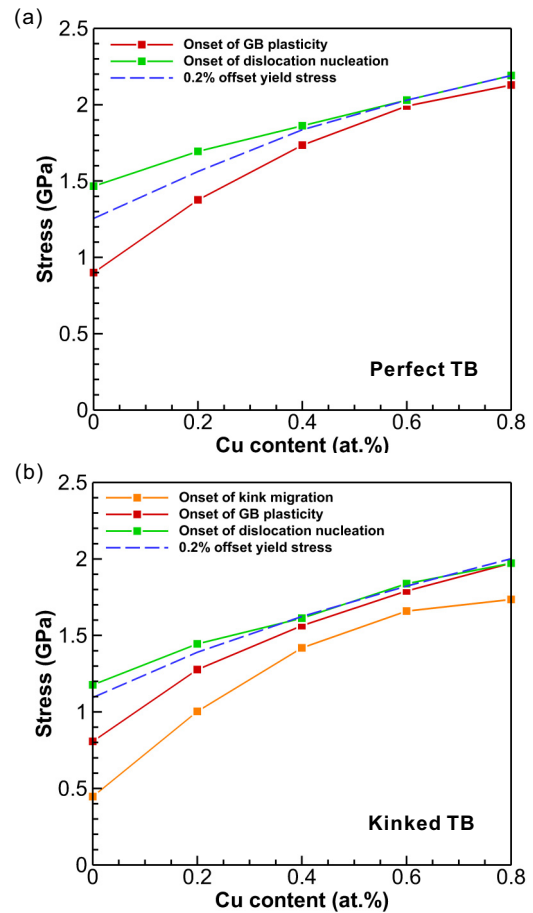


FIG. 5. Dependence of yield strength on Cu doping in nt-Ag containing (a) perfect TBs and (b) kinked TBs.

Fig. 6. Figures 6(a)–6(c) show that undoped bicrystals are predominantly deformed by kink annihilation through step migration at approximately the same stress under all shear loading conditions. However, Fig. 6(d) suggests pronounced Cu segregation strengthening up to 0.75 at. % Cu, followed by a plateau at constant strength for higher dopant concentrations. Simultaneously, the yielding mechanism of TB kink steps is found to change from defect migration to nucleation of lattice dislocations in the form of either in-plane kink splitting or inclined 60° dislocation, as indicated by S and N symbols, respectively.

## IV. DISCUSSION

A major finding of this study is that both twin stability and yield strength in nt-Ag metals are proven to increase substantially by introducing trace concentrations of Cu solute atoms. A striking feature discovered in our simulations is the importance of dilute Cu atoms segregating toward intrinsic TB kink-step defects, together with classical GB segregation. Periodic segregation of rare-earth Gd solute atoms at fully coherent TBs has been observed in a recent experimental study in hexagonal-close-packed Mg alloys [42]. These TBs were formed by deformation twinning, and solute atom segregation acted to relieve the residual elastic strain caused by local compression sites. On the contrary, coherent TB segments in
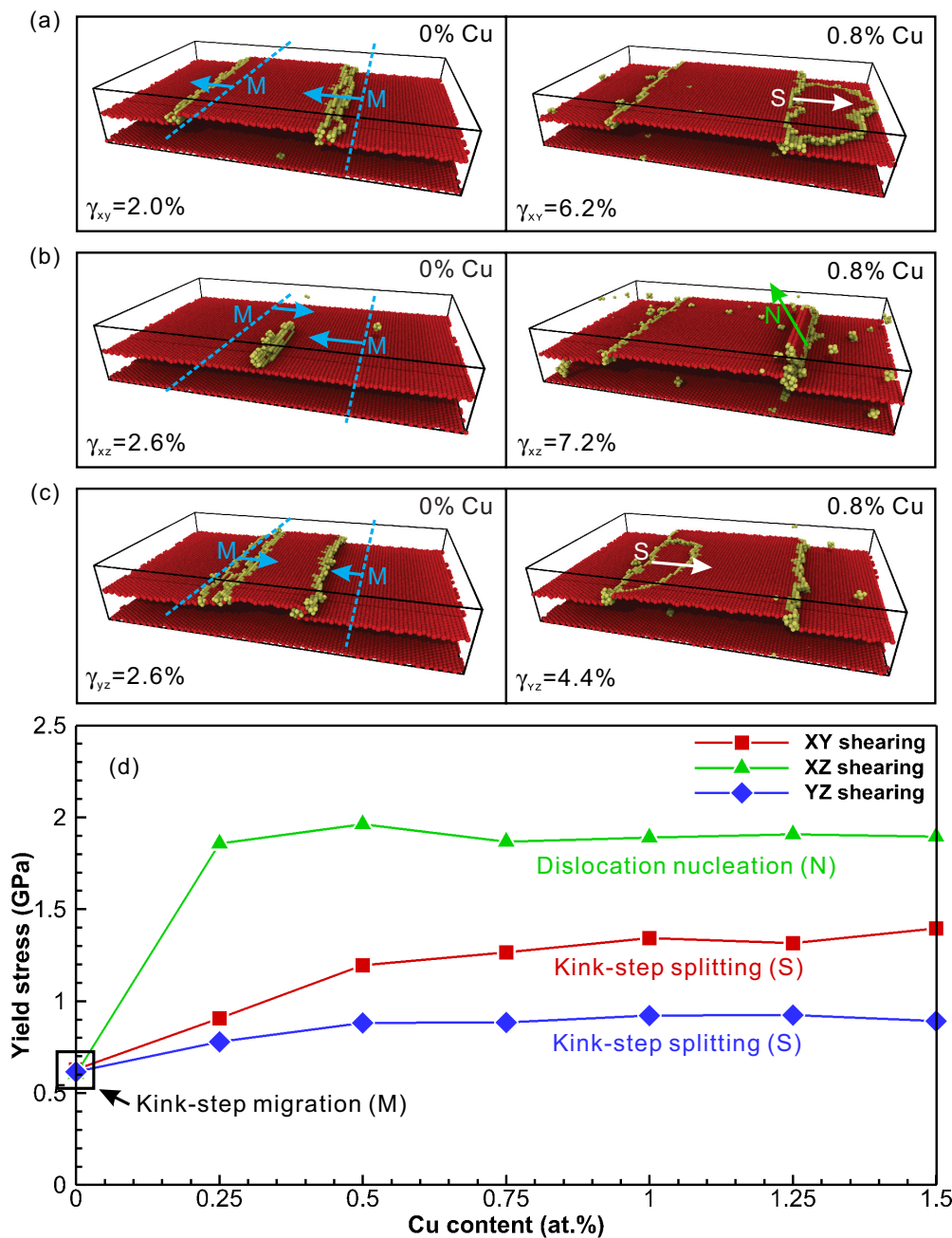
FIG. 6.  Intrinsic Cu segregation effects on plastic yielding of a twin-boundary kink defect in GB-free kinked bicrystals subjected to pure shear loading on different planes. (a)–(c) Yielding mechanisms with and without Cu doping for shearing in either $xy$, $xz$, or $yz$ shear planes. (d) Critical yield stress as a function of segregated Cu content.

the present nt-Ag models were fully relaxed and strain-free, and thus their role was found to be inconsequential for equilibrium Cu segregation. Therefore, solute atom segregation to TB defects in nt-Ag can be viewed as significant in several aspects.

First, it demonstrates that Cu segregation by microalloying can directly impact twin stability in nt-Ag in the absence of solid solution strengthening. TB kink steps are made of three dislocations whose Burgers vector sum is null. So, this type of defect can easily glide in full along TBs at low applied shear stress, giving rise to permanent detwinning by step annihilation or absorption at GBs, as shown in Fig. 4(d) and Movie S1 [41].

The present study shows that the pinning of TB kink steps due to atom segregation is central to twin stability. Apparently, similar atomic processes were recently observed in $\alpha$-Fe where dislocations were found to be strongly pinned by substitutional He segregation [43]. As shown in Fig. 6, with less than 1 at. % Cu concentration, the critical shear stress to plastically deform a kink defect in a bicrystal can be increased by a factor between 33 and 200%, depending on the loading direction. In large-scale polycrystal models, the tensile stress at twin instability was remarkably increased by more than 300% at 0.8 at. % Cu. In pure nt-Ag metals synthesized experimentally, the smallest TB spacing reported so far has been ∼8 nm [28–30].

The above theoretical predictions, however, suggest that even smaller TB spacings could possibly be achieved in this metal by microalloying.

Second, low Cu concentrations ($\leqslant 0.8$ at. %) were found to efficiently increase the overall yield strength by 83% from that of undoped models with identical microstructures. This result is significant with respect to previous studies on GB strengthening effects from dilute atom segregation in the Cu-Ag alloy system. Vo *et al.* [17], using the same simulation approach as here, described that the yield strength of nc-Cu increased by only 15% by GB doping with 0.8 at. % Ag. Also, with similar local concentrations in GBs, Li and Szlufarska [27] simulated that the 0.2% offset yield stress increased by 23% in nc-Cu by Ag doping, with a grain size of 40 nm, close to that examined in the present models. This comparison therefore implies that GB strengthening alone cannot entirely account for the exceptional strengthening observed in the present study, and that other Cu-dependent strengthening mechanisms could be at play.

Third, offset yield stresses in large-scale nt-Ag polycrystals with different Cu concentrations were found to closely match the segregated Cu dependence of critical stress to initiate crystal slip in nt-Ag models with both perfect and imperfect TBs. This observation provides numerical evidence that dislocation emission is the dominant yielding mechanism in this material. We find GB sliding to be a precursor for dislocation nucleation, which is in agreement with past atomistic simulations of incipient plasticity in nc metals [34]. The same mechanism is predicted to hold with Cu doping, albeit the stress difference at the onsets of GB sliding and crystal slip is dramatically reduced with increasing dopant concentration. This can be attributed to the role of atom segregation in decreasing the excess free volume at GBs. This phenomenon was studied in nc Ni-Fe and Cu-Ag alloys [18,27], where a direct relationship between segregation affected excess GB free volume and offset yield stress was proposed. The finding that GB-mediated dislocation nucleation is distributed and not site-specific tends to support this hypothesis. Another interesting result obtained here is that TB kink steps become primary nucleation sites for crystal slip at yielding, in addition to GB-mediated dislocation nucleation. As such, this study presents a type of yield stress dependence on atom segregation based on Cu affected dislocation emission from TB defects.

## V. CONCLUSION

Hybrid MC/MD simulations have been used to study the atomic processes of Cu segregation in microalloyed nt-Ag metals. A major conclusion is that both twin stability and yield strength in nt-Ag metals are increased substantially by introducing trace concentrations of Cu solute atoms less than 1 at. %. Preferential segregation of Cu atoms toward intrinsic TB kink steps was found to promote twin stability and resistance to detwinning by pinning of TB defects, alongside classical GB segregation. In addition to GB strengthening, doping is found to fundamentally change the plastic deformation of TB defects from migration to kink-activated crystal slip. It was shown that yield strength is directly associated with the Cu-dependent critical stress for dislocation nucleation at GBs and TB defects. This study suggests that microalloying may enable the design of new nt metals with superior strengths and structure stability that could potentially exceed the current limits.

[1] D. C. Bufford, Y. M. Wang, Y. Liu, and L. Lu, MRS Bull. **41**, 286 (2016).

[2] L. Lu, X. Chen, X. Huang, and K. Lu, Science **323**, 607 (2009).

[3] Y. S. Lei Lu, X. Chen, L. Qian, and K. Lu, Science **304**, 422 (2004).

[4] O. Anderoglu, A. Misra, H. Wang, F. Ronning, M. F. Hundley, and X. Zhang, Appl. Phys. Lett. **93**, 083108 (2008).

[5] Y. Zhao, T. A. Furnish, M. E. Kassner, and A. M. Hodge, J. Mater. Res. **27**, 3049 (2012).

[6] Y. Zhao, I. Cheng, M. Kassner, and A. Hodge, Acta Mater. **67**, 181 (2014).

[7] A. Stukowski, K. Albe, and D. Farkas, Phys. Rev. B **82**, 224103 (2010).

[8] X. Li, Y. Wei, L. Lu, K. Lu, and H. Gao, Nature (London) **464**, 877 (2010).

[9] Z. You, X. Li, L. Gui, Q. Lu, T. Zhu, H. Gao, and L. Lu, Acta Mater. **61**, 217 (2013).

[10] F. Sansoz, K. Lu, T. Zhu, and A. Misra, MRS Bull. **41**, 292 (2016).

[11] Y. M. Wang, F. Sansoz, T. LaGrange, R. T. Ott, J. Marian, T. W. Barbee, Jr., and A. V. Hamza, Nat. Mater. **12**, 697 (2013).

[12] N. Lu, K. Du, L. Lu, and H. Q. Ye, Nat. Commun. **6**, 7648 (2015).

[13] Q. Fang and F. Sansoz, Acta Mater. **123**, 383 (2017).

[14] L. Xu, D. Xu, K. N. Tu, Y. Cai, N. Wang, P. Dixit, J. H. L. Pang, and J. Miao, J. Appl. Phys. **104**, 113717 (2008).

[15] A. Caro, D. Farkas, E. Bringa, G. Gilmer, and L. Zepeda-Ruiz, in *Materials Science Forum* (Trans. Tech Publishing, Switzerland, 2010), p. 21.

[16] J. Schäfer, A. Stukowski, and K. Albe, Acta Mater. **59**, 2957 (2011).

[17] N. Q. Vo, J. Schäfer, R. S. Averback, K. Albe, Y. Ashkenazy, and P. Bellon, Scr. Mater. **65**, 660 (2011).

[18] J. Schafer and K. Albe, Beilstein J. Nanotechnol. **4**, 542 (2013).

[19] P. Zhang, J. Y. Zhang, J. Li, G. Liu, K. Wu, Y. Q. Wang, and J. Sun, Acta Mater. **76**, 221 (2014).

[20] Y. Zhang, G. J. Tucker, and J. R. Trelewicz, Acta Mater. **131**, 39 (2017).

[21] S. C. Pun, W. Wang, A. Khalajhedayati, J. D. Schuler, J. R. Trelewicz, and T. J. Rupert, Mater. Sci. Eng. **696**, 400 (2017).

[22] J. Schäfer, Y. Ashkenazy, K. Albe, and R. S. Averback, Mater. Sci. Eng. **546**, 307 (2012).

[23] M. Kapoor, T. Kaub, K. A. Darling, B. L. Boyce, and G. B. Thompson, Acta Mater. **126**, 564 (2017).

[24] S. Özerinç, K. Tai, N. Q. Vo, P. Bellon, R. S. Averback, and W. P. King, Scr. Mater. **67**, 720 (2012).

[25] H. W. Zhang, K. Lu, R. Pippan, X. Huang, and N. Hansen, Scr. Mater. **65**, 481 (2011).

[26] G. Kim, X. Chai, L. Yu, X. Cheng, and D. S. Gianola, Scr. Mater. **123**, 113 (2016).

[27] A. Li and I. Szlufarska, J. Mater. Sci. **52**, 4555 (2017).

[28] D. Bufford, H. Wang, and X. Zhang, Acta Mater. **59**, 93 (2011).

[29] T. Furnish and A. Hodge, APL Mater. **2**, 046112 (2014).

[30] R. Ott, J. Geng, M. Besser, M. Kramer, Y. Wang, E. Park, R. LeSar, and A. King, Acta Mater. **96**, 378 (2015).

[31] A. Detor and C. Schuh, Acta Mater. **55**, 4221 (2007).

[32] S. Plimpton, J. Comput. Phys. **117**, 1 (1995).

[33] H. H. Wu and D. R. Trinkle, Comput. Mater. Sci. **47**, 577 (2009).

[34] F. Sansoz and K. D. Stevenson, Phys. Rev. B **83**, 224101 (2011).

[35] J. Wang, N. Li, O. Anderoglu, X. Zhang, A. Misra, J. Y. Huang, and J. P. Hirth, Acta Mater. **58**, 2262 (2010).

[36] B. Sadigh, P. Erhart, A. Stukowski, A. Caro, E. Martinez, and L. Zepeda-Ruiz, Phys. Rev. B **85**, 184203 (2012).

[37] D. Bufford, H. Wang, and X. Zhang, J. Mater. Res. **28**, 1729 (2013).

[38] A. Stukowski, Modell. Simul. Mater. Sci. Eng. **18**, 015012 (2010).

[39] G. Voronoi, J. Reine Angew. Math. **138**, 198 (1908).

[40] J. Towns *et al.*, Comput. Sci. Eng. **16**, 62 (2014).

[41] See Supplemental Material at http://link.aps.org/supplemental/10.1103/PhysRevMaterials.1.063604 for movies of MD simulation of plastic yielding up to 3% applied strain in undoped nt-Ag containing perfect coherent TBs (Movie S1), undoped nt-Ag containing imperfect kinked TBs (Movie S2), and doped nt-Ag with 0.8 at. % Cu containing imperfect kinked TBs (Movie S3). The time interval between two snapshots is 5 ps.

[42] J. F. Nie, Y. M. Zhu, J. Z. Liu, and X. Y. Fang, Science **340**, 957 (2013).

[43] E. Martínez, D. Schwen, and A. Caro, Acta Mater. **84**, 208 (2015).